

Nanoptera and Stokes Curves in the 2-Periodic Fermi-Pasta-Ulam-Tsingou Equation

C. J. Lustri^{1*}

¹Department of Mathematics and Statistics, 12 Wally's Walk, Macquarie University, New South Wales 2109, Australia

Abstract

This work presents asymptotic solutions to a singularly-perturbed, period-2 FPUT lattice and uses exponential asymptotics to examine ‘nanoptera’, which are nonlocal solitary waves with constant-amplitude, exponentially small wave trains which appear behind the wave front. Using an exponential asymptotic approach, this work isolates the exponentially small oscillations, and demonstrates that they appear as special curves in the analytically-continued solution, known as ‘Stokes curves’ are crossed. By isolating these the asymptotic form of these oscillations, it is shown that there are special mass ratios which cause the oscillations to vanish, producing localized solitary-wave solutions. The asymptotic predictions are validated through comparison with numerical simulations.

Keywords: solitary waves, exponential asymptotics, nanoptera, FPUT lattice

AMS Subject Classifications: 34E15, 35Q51, 34C15, 37K60

1 Introduction

In this study, we demonstrate the important role played by Stokes phenomenon in the behaviour of travelling waves propagating through a diatomic Fermi-Pasta-Ulam-Tsingou (FPUT) lattice. The classical FPUT lattice contains an infinitely long line of masses connected to their neighbours by identical springs. After non-dimensionalization, this system can be represented by

$$m(j)\ddot{x}(j,t) = F(x(j+1,t) - x(j,t)) - F(x(j,t) - x(j-1,t)), \quad (1)$$

where $x(j,t)$ represents the position of the j th particle at time t , a dot refers to differentiation with respect to time, and F is an interaction potential given by

$$F(r) = r + r^2. \quad (2)$$

A diatomic lattice has $m(j) = m_1$ if j is odd, and $m(j) = m_2$ if j is even, where $m_1 \neq m_2$. This system has a speed of sound given by $c_0 = \sqrt{2/(m_1 + m_2)}$. In this study, we are interested in the behaviour of supersonic travelling waves (with speed $c_\epsilon > c_0$) in diatomic systems with small mass ratio. We therefore set δ such that $m_2/m_1 = \delta^2$ with $0 < \delta \ll 1$.

The behaviour of travelling waves in monoatomic FPUT lattice has been treated comprehensively in, for example, [19, 20, 21]. These studies determined that the travelling wave solution is a localized solitary wave that is a regular perturbation away from a solution to the Kortweg-de Vries (KdV) equation in the long-wave asymptotic

*Electronic address: christopher.lustri@mq.edu.au

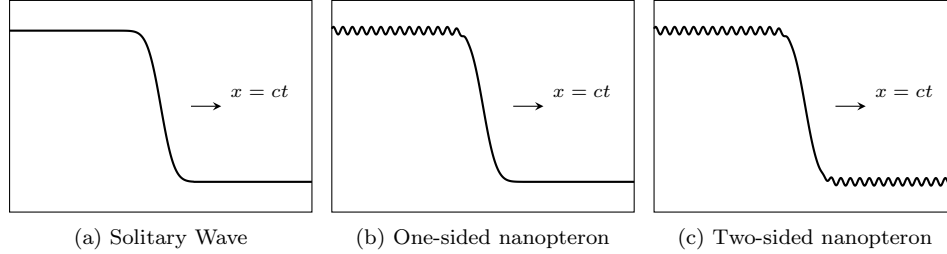


Figure 1: Comparison of the profiles associated with (a) a standard solitary wave, (b) a one-sided nanoopteron, and (c) a two-sided nanoopteron that each propagate at speed c . The solitary wave is localized spatially, whereas the nanoptera have non-decaying oscillatory tails on (b) one side or (c) both sides of the wave front.

limit. These studies led to the natural question of whether the results could be generalized to polyatomic FPUT lattices, and how travelling waves would propagate through such systems.

In a later analysis, Gaison *et al.* [22] found that the equations governing travelling waves in diatomic FPUT systems can be written as a singular, rather than regular, perturbation to a solution to the KdV equation. The KdV solution is a long-wave approximation that depends on a small parameter, and the solution is accurate up to algebraic order in this parameter. We will later use this KdV solution as a leading-order solution to the diatomic FPUT lattice equation (1) in the small mass ratio limit. A number of other rigorous and formal studies of the behaviour of periodic lattice systems have been undertaken in the past, including [13, 33, 34, 36, 42].

Faver & Wright [17] and Hoffman & Wright [24] used a Beale ansatz (introduced in [1]) to rigorously prove the existence of supersonic travelling wave solutions in the diatomic FPUT lattice, which are composed of the sum of an exponentially localized solitary wave and periodic oscillations with exponentially small amplitude. Solutions of this form are known as ‘nanoopteron’ solutions. Boyd introduced the term ‘nanoopteron’ in [8] to describe weakly nonlocal solitary waves, which approximately satisfy the classical definition of a solitary wave with the distinction that a nanoopteron wave is not exponentially localized, but rather tends to a small-amplitude oscillation on either one or both sides of the central solitary wave, illustrated in Figure 1.

Nanoopteron solutions to the diatomic FPUT lattice equation were directly observed in the numerical study [23], which investigated the question of whether such waves are metastable (that is, stable up to a slow erosion due to the formation of the oscillatory wavetrain). This study presented the numerical technique used in Section 5 to validate the formal asymptotic analysis.

A number of other studies have been performed on diatomic FPUT (or related) lattices. Qin [35] proved the existence of periodic supersonic wavetrains in such a lattice, which correspond to the far-field periodic oscillations far from the travelling wave front in the present study. Faver later used a Beale ansatz to prove the existence of nanoopteron solutions in FPUT lattices with 2-periodic spring potential (2), rather than the 2-periodic mass considered here.

Previous mathematical and experimental studies of lattices with periodic masses have revealed dynamics which do not arise in uniform lattices [25, 26, 31, 34, 38, 39]. In particular, diatomic lattices permit new families of solitary waves which can exist only for discrete values of the ratio between the masses of the two particles in a diatomic unit [25, 26, 39]. In [25], these ratios are described as anti-resonances. Asymptotic descriptions of these mass ratios for the diatomic Toda lattice were first obtained in [39] using a matched asymptotic expansion technique, and explained in [30] as destructive interference between two distinct exponentially small wavetrains in the solution. This study exploited the asymptotic form of the exponentially small terms to find a simplified asymptotic expression for the mass ratios that produce cancellation.

This paper uses an adaptation of the technique developed in [30] for studying travelling waves in a diatomic Toda lattice with small mass ratio. This previous work found that travelling waves in the diatomic Toda are nanoptera, and that the exponentially small oscillations appear as curves in the complex plane known as ‘Stokes

curves’, discussed in Section 1.1. In the present study, we show that corresponding behaviour is found in supersonic travelling wave solutions for the diatomic FPUT lattice with small mass ratio. We will also show that the special nanopteron-free asymptotic solutions – true solitary waves – computed in [30, 39] are also present in the diatomic FPUT lattice, and are caused by destructive interference between two distinct oscillatory contributions.

In the present work, we do not obtain a rigorous existence proof, and we instead take a similar approach to [30, 39] and compare the results of our formal analysis to computational results. In this study, we use exponential asymptotic techniques developed by [12, 32] to provide a mathematical description of nanopteron solutions in the period-2 FPUT lattice.

The remainder of this paper is organized as follows. The method of exponential asymptotics is introduced in Section 1.1. The equations for diatomic FPUT lattices are shown in Section 2, the long wave approximation to the solution is provided. In Section 3, the solutions to the FPUT equations are expanded as asymptotic power series in the small mass ratio. The leading-order behaviour of this series is found in Section 3.1, and an ansatz is applied to determine the late-order behaviour in Section 3.2, with some technical details found in Appendix A. A full exponential asymptotic analysis is performed in Section 4. This involves finding the Stokes structure of the solution in 4.1, and determining the asymptotic form of the exponentially small oscillations in Section 4.2. In Section 5, the asymptotic results are compared to numerical simulations, and it is noted that nanopteron-free solutions are apparent in both the numerical and asymptotic results. In Section 6, an asymptotic expression is obtained for the special mass ratios that produce nanopteron-free solutions. The paper concludes in Section 7.

1.1 Exponential Asymptotics

We examine the asymptotic behavior of exponentially small, non-decaying waves that appear in the wake of a solitary-wave front in diatomic FPUT lattices. However, determining the behavior of terms that are exponentially small compared to the leading-order solution in the $\epsilon \rightarrow 0$ asymptotic limit is impossible using classical asymptotic series expansions, because the exponentially small contribution is necessarily smaller than any power of the small parameter δ . Therefore, we apply specialized techniques, known as ‘exponential asymptotics’, to determine behavior on this scale [9, 10]. This section contains a brief outline of the method that will be used in the present study, adapted from the description in [30].

As we uncover this exponentially small behavior, we will see that the analytic continuation of the asymptotic solution includes curves known as ‘Stokes curves’ [37]. These curves are related to the behavior of exponentially small contributions to the solutions. As a Stokes curve is crossed, the exponentially small contribution experiences a smooth, rapid change in value in the neighborhood of the curve. In many problems, including the present investigation, the exponentially small contribution to the solution appears only on one side of a Stokes curve.

The central idea of exponential asymptotic methods is that a divergent asymptotic series may be truncated to approximate the exact solution. Furthermore, one can choose the truncation point to minimize the error between the approximation and the exact solution; this is known as ‘optimal truncation’. When a divergent series is truncated optimally, the approximation error is generally exponentially small in the asymptotic limit [10]. The problem may then be rescaled to directly determine this approximation error, allowing the exponentially small component of the solution to be determined in the absence of the asymptotic series itself. This idea was introduced by Berry [4, 5], and it was employed in [3, 6] to determine the position of Stokes curves, and associated switching behaviour in special functions such as the Airy function.

In the present paper, we apply an exponential asymptotic method developed by Olde Daalhuis et al. [32] for linear differential equations and extended by Chapman et al. [12] to nonlinear ordinary differential equations. Here we provide a brief outline of the process; see the above papers for a more detailed explanation of the methodology.

The first step in exponential asymptotic analysis is to express the solution as an asymptotic power series. In many singular perturbation problems, including the problem considered in the present study, the asymptotic

series solution diverges. For a more detailed discussion of asymptotic series divergence, see [11, 15]. Optimally truncating these divergent series typically requires a general form for the asymptotic series coefficients, and it is frequently algebraically intractable to obtain such a general form. In practice, however, one does not require the exact form of the series coefficients. Instead, one needs only the so-called ‘late-order terms’, or asymptotic expressions for the r th series coefficient in the $r \rightarrow \infty$ limit.

Dingle [15] noted that the terms of the divergent asymptotic power series of a singularly perturbed system are typically obtained by repeated differentiations, and therefore diverge in a predictable factorial-over-power fashion. Noting this observation, Chapman et al. [12] proposed writing an ansatz for the late-order terms that is capable of describing this form of late-order term behavior. One can write an ansatz for the r th term of a divergent asymptotic series (denoted g_r) as $r \rightarrow \infty$ using the form

$$g_r \sim \frac{G\Gamma(r + \gamma)}{\chi^{r+\gamma}} \quad \text{as } r \rightarrow \infty, \quad (3)$$

where G , γ , and χ are functions that do not depend on r but are free to vary with independent variables (and hence with z). The ‘singulant’ χ equals 0 at values of z , denoted by $z = z_s$, at which the leading-order behavior g_0 is singular. This ensures that the late-order ansatz for g_r also has a singularity at $z = z_s$ and that the singularity increases in strength as r increases. One can then use the ansatz (3) to optimally truncate an asymptotic expansion. The method developed in Olde Daalhuis et al. [32] involves substituting the resulting truncated series expression into the original problem to obtain an equation for the exponentially small remainder term.

The exponentially small contribution to the asymptotic solution that one obtains using the above method, denoted g_{exp} , generally takes the form in the limit $\delta \rightarrow 0$ given by

$$g_{\text{exp}} \sim \mathcal{S}G e^{-\chi/\delta}, \quad (4)$$

where the ‘Stokes multiplier’ \mathcal{S} varies rapidly from 0 to a nonzero value as one crosses a Stokes curve. This behavior is known as ‘Stokes switching’, and it occurs along curves at which the switching exponential is maximally subdominant and hence where the singulant χ is real and positive [6]. The variation is smooth, and it occurs in a neighborhood of width $\mathcal{O}(\sqrt{\delta})$ that contains the Stokes curve.

This primary advantages of this approach are that it reveals the important role played by the Stokes curves in the asymptotic solution, and it does not require the computation of terms beyond the leading-order expression to obtain the form of exponentially small correction terms. The latter of these advantages makes the technique particularly useful for the many nonlinear problems for which obtaining even these low-order correction terms is intractable. See the review article [10] or monograph [9] for more details on exponential asymptotics and their application to nonlocal solitary waves, [4, 5, 11] for examples of previous studies of exponential asymptotics, and [12, 32] for more details on the particular methodology that we apply in the present paper.

2 Diatomic FPUT Equation

We consider the diatomic FPUT lattice equations given in (1)–(2), with $m(j) = m_1$ for j odd, and $m(j) = m_2$ for j even. We express the mass ratio as $\delta = \sqrt{m_2/m_1}$, and set $0 < \delta \ll 1$.

Long waves with small amplitudes in diatomic FPUT lattices were previously studied in [22] in terms of the offset $r(j, t)$ and the particle velocity $p(j, t)$, defined by

$$r(j, t) = x(j + 1, t) - x(j, t), \quad p(j, t) = \dot{x}(j, t). \quad (5)$$

In [22], a long-wave solution was found in terms of a small parameter ϵ that specifies the amplitude and width of the travelling wave. The long-wave solution was given by

$$(r(j, t), p(j, t)) = 3\epsilon^2 \text{sech}^2(\beta\epsilon(j - c_\epsilon t))(1, -c_0) + \mathcal{O}(\epsilon^{5/2}), \quad (6)$$

in the limit that $\epsilon \rightarrow 0$, where

$$\beta = \sqrt{\frac{3(m_1^2 + 2m_1m_2 + m_2^2)}{2(m_1^2 - m_1m_2 + m_2^2)}}, \quad c_\epsilon = (1 + \epsilon^2)\sqrt{\frac{2}{m_1 + m_2}}. \quad (7)$$

We see that small ϵ corresponds to a long, small-amplitude travelling wave moving at slightly above the speed of sound in the system, c_0 . By integrating the particle velocities, we obtain

$$x(j, t) = \frac{3\epsilon}{\beta} \tanh(\beta\epsilon(j - c_\epsilon t)) + \mathcal{O}(\epsilon^{3/2}). \quad (8)$$

This approximate travelling wave solution will play an important role in subsequent analysis.

For clarity in subsequent analysis, we will denote the position of the heavier particles as $y(j, t)$ where j takes odd values, and the lighter particles as $z(j, t)$ where j takes even values. It is always possible to remove the larger mass through non-dimensionalizing the system, so without any loss of generality, we set $m_1 = 1$ and $m_2 = \delta^2$ in all subsequent analysis. We are interested in travelling wave solutions, and hence convert to a moving frame, such that $y(j, t) = y(\xi)$ and $z(j, t) = z(\xi)$. The governing equations become

$$c_\epsilon^2 y''(\xi) = F(z(\xi + 1) - y(\xi)) - F(y(\xi) - z(\xi - 1)), \quad j \text{ odd}, \quad (9)$$

$$\delta^2 c_\epsilon^2 z''(\xi) = F(y(\xi + 1) - z(\xi)) - F(z(\xi) - y(\xi - 1)), \quad j \text{ even}, \quad (10)$$

where a dash denotes a derivative with respect to ξ .

Before considering the behaviour of this system for small δ , we must determine whether the $\delta = 0$ system contains exponentially small oscillations in the far field due to the discrete nature of the system itself, such as those seen for the discretized Korteweg-de Vries (KdV) equation in [27]. It is straightforward to see that when $\delta = 0$, the governing equations become

$$c_\epsilon^2 y''(\xi) = F(\tfrac{1}{2}(y(\xi + 2) - y(\xi))) - F(\tfrac{1}{2}(y(\xi) - y(\xi - 2))), \quad j \text{ odd}, \quad (11)$$

$$z(\xi) = \tfrac{1}{2}y(\xi + 1) + \tfrac{1}{2}y(\xi - 1), \quad j \text{ even}. \quad (12)$$

This shows that the position of the heavy particles is governed by a scaled monoatomic FPUT equation, while the lighter particles occupy the average position of their nearest neighbours. From previous work including [19, 20, 21], we know that travelling waves in the monoatomic FPUT lattice are localized solitary waves. Consequently, the long-wave approximation to the $\delta = 0$ system does not introduce exponentially small far-field oscillations. This confirms that any far-field oscillations in solutions to the full system (9)–(10) are introduced by the singular perturbation caused by the small mass ratio parameter δ .

3 Series Expansion

We expand the dependent variables as a Taylor series in δ , giving

$$y(\xi) = \sum_{r=0}^{\infty} \delta^{2r} y_r(\xi), \quad z(\xi) = \sum_{r=0}^{\infty} \delta^{2r} z_r(\xi), \quad (13)$$

where the coefficients y_r and z_r depend on the long-wave parameter ϵ , but not the mass ratio δ . We may determine equations for the coefficients by applying these series expressions to (9)–(10), and matching in the limit that $\delta \rightarrow 0$.

3.1 Leading-order series terms

At leading order in the limit that $\delta \rightarrow 0$, this gives

$$c_\epsilon^2 y_0''(\xi) = F(z_0(\xi + 1) - y_0(\xi)) - F(y_0(\xi) - z_0(\xi - 1)), \quad j \text{ odd}, \quad (14)$$

$$0 = F(y_0(\xi + 1) - z_0(\xi)) - F(z_0(\xi) - y_0(\xi - 1)), \quad j \text{ even}. \quad (15)$$

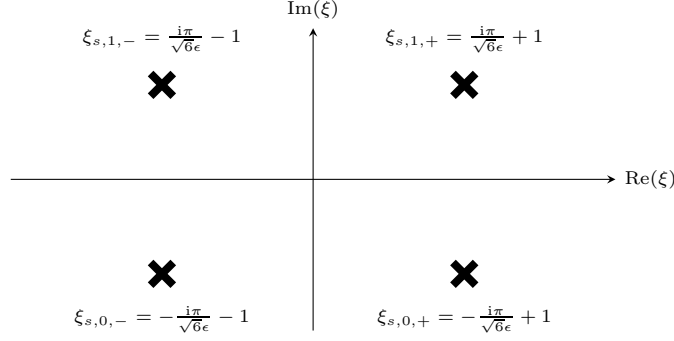


Figure 2: Singularities of $z_0(\xi)$ given by (18) that will contribute to the asymptotic form of the far-field oscillations. The subsequent analysis for the oscillations due to the singularity at $\xi = \xi_{s,1,-}$, denoted ξ_s , will be shown in detail. The remaining three singularity contributions will be subsequently stated.

This is equivalent to the full diatomic FPUT system (1) with $\delta = 0$. Consequently, we may construct an approximate travelling wave solution may be found by setting $m_1 = 1$ and $m_2 = 0$ in (6). This gives the long-wave solution in the limit that $\epsilon \rightarrow 0$ as

$$y_0(\xi) = \sqrt{6}\epsilon \tanh\left(\sqrt{\frac{3}{2}}\epsilon\xi\right) + \mathcal{O}(\epsilon^{3/2}), \quad z_0(\xi) = \frac{1}{2}(y(\xi+1) + y(\xi-1)), \quad (16)$$

where $y_0(\xi)$ and $z_0(\xi)$ take odd and even values of j respectively. There is a significant difference at this stage between the present analysis of the diatomic FPUT lattice, and the analysis of the diatomic Toda lattice from [27]; in the analysis of the Toda lattice, the leading order solution is known exactly, whereas for the FPUT lattice, it is approximated up to $\mathcal{O}(\epsilon^{3/2})$. Consequently, we have two small parameters in the system, which introduces an extra source of error into the approximation.

Finally, for the purposes of subsequent analysis, it is important to observe that the expression for $z_0(\xi)$ is singular at $\xi = \xi_{s,N,\pm}$ where

$$\xi_{s,N,\pm} = \frac{(2N-1)\pi i}{\sqrt{6}\epsilon} \pm 1, \quad N \in \mathbb{Z}, \quad (17)$$

and that the singular behaviour is given by

$$z(\xi) \sim (\xi - \xi_{s,N,\pm})^{-1} \quad \text{as} \quad \xi \rightarrow \xi_{s,N,\pm}, \quad (18)$$

for any choice of $N \in \mathbb{Z}$ and sign.

We need only consider the contributions associated with singularities nearest to the real axis, or $N = 1$ and $N = 0$. In all subsequent analysis, we will consider the exponentially small oscillations caused by the singularity in $z_0(\xi)$ at $\xi = \xi_{s,1,-}$. For simplicity of notation, we will denote this particular choice as $\xi = \xi_s$ in subsequent analysis, giving $\xi_s = \pi i/\sqrt{6}\epsilon - 1$.

The contributions associated with singularities at $\xi = \xi_{s,0,-}$, $\xi_{s,1,+}$, and $\xi_{s,0,+}$ will also contribute to the asymptotic form of the far-field oscillations, and the corresponding results will be stated after the conclusion of the detailed analysis for $\xi = \xi_s$. The four singularities are illustrated in Figure 2.

3.2 Late-order series terms

The recursion relation is obtained by applying the series expression (13) to the governing equations (9)–(10) and matching orders of δ , giving

$$c_\epsilon^2 y_r''(\xi) = (z_r(\xi+1) - y_r(\xi))F'(z_0(\xi+1) - y_0(\xi)) - (y_r(\xi) - z_r(\xi-1))F'(y_0(\xi) - z_0(\xi-1)) + \dots, \quad (19)$$

$$c_\epsilon^2 z_r''(\xi) = (z_r(\xi+1) - y_r(\xi))F'(z_0(\xi+1) - y_0(\xi)) - (y_r(\xi) - z_r(\xi-1))F'(y_0(\xi) - z_0(\xi-1)) + \dots, \quad (20)$$

where the omitted terms will be smaller than those retained in the limit that $r \rightarrow \infty$.

In principle this recursion relation could be repeatedly applied in order to obtain subsequent terms in the series; however this is technically challenging, and it will not reveal the presence of exponentially small oscillations in the far-field, as such oscillations are typically exponentially small in the singularly perturbed limit ($\delta \rightarrow 0$).

Instead, we must follow [30] and determine the asymptotic form of the series terms in the limit that $r \rightarrow \infty$, known as the late-order terms. We see that obtaining the value of y_r and z_r for large r requires two differentiations of the term z_{r-1} . Hence, we can follow the process devised in Chapman et al. [12] and apply a factorial-over-power late-order ansatz to approximate these terms as $r \rightarrow \infty$.

The required ansatz takes the form

$$y_r(\xi) \sim \frac{Y(\xi)\Gamma(2r + \alpha)}{\chi(\xi)^{2r+\alpha}}, \quad z_r(\xi) \sim \frac{Z(\xi)\Gamma(2r + \beta)}{\chi(\xi)^{2r+\beta}}, \quad \text{as } r \rightarrow \infty. \quad (21)$$

An identical balancing argument to the equivalent analysis for the diatomic Toda lattice from [30] gives $\alpha = \beta - 2$. Substituting the late-order terms (21) into the recursion relation (20) and keeping only the first two orders in the large r limit gives

$$\begin{aligned} \frac{c_\epsilon^2(\chi')^2 Z \Gamma(2r + \alpha)}{\chi^{2r+\alpha}} - \frac{2c_\epsilon^2 \chi' Z' \Gamma(2r + \alpha - 1)}{\chi^{2r+\alpha-1}} - \frac{c_\epsilon^2 \chi'' Z \Gamma(2r + \alpha - 1)}{\chi^{2r+\alpha-1}} \\ = -\frac{2Z \Gamma(2r + \alpha)}{\chi^{2r+\alpha}} F'(\tfrac{1}{2}(y_0(\xi + 1) - y_0(\xi - 1))) + \dots, \end{aligned} \quad (22)$$

where we use the leading-order relationship between $y_0(\xi)$ and $z_0(\xi)$, and the omitted terms are smaller than those retained as $r \rightarrow \infty$.

3.2.1 Calculating χ

Matching (22) at $\mathcal{O}(z_r)$ as $r \rightarrow \infty$, we find that

$$c_\epsilon^2(\chi')^2 = -2(1 + y_0(\xi + 1) - y_0(\xi - 1)). \quad (23)$$

Integrating this, and recalling that $\chi = 0$ and the singularity location $\xi = \xi_s$ gives

$$\chi = \pm \frac{i\sqrt{2}}{c_\epsilon} \int_{\xi_s}^{\xi} \sqrt{1 + y_0(\xi + 1) - y_0(\xi - 1)} ds. \quad (24)$$

The integral contour is depicted in Figure 3. While any contour may be chosen, it is helpful to divide the contour into a vertical component \mathcal{C}_1 and a horizontal component \mathcal{C}_2 . The real contribution to this integral arises by integrating down \mathcal{C}_1 , while the imaginary contribution is caused by integrating along \mathcal{C}_2 .

Consequently, this allows us to obtain the real and imaginary parts of the singulant,

$$\text{Re}(\chi) = \pm \frac{i\sqrt{2}}{c_\epsilon} \int_{\mathcal{C}_1} \sqrt{1 + y_0(\xi + 1) - y_0(\xi - 1)} ds, \quad \text{Im}(\chi) = \pm \frac{\sqrt{2}}{c_\epsilon} \int_{\mathcal{C}_2} \sqrt{1 + y_0(\xi + 1) - y_0(\xi - 1)} ds. \quad (25)$$

We note that $\text{Re}(\chi)$ is constant for real ξ , which causes the far field oscillations to have constant amplitude.

For Stokes switching to occur, we recall from Section 1.1 that $\text{Re}(\chi) > 0$, which corresponds to the positive choice of sign. Hence, we restrict our subsequent analysis to this sign choice.

It will be important in the subsequent analysis to know the local behaviour of the singulant near the singular point. It is straightforward to show by direct computation that

$$c_\epsilon^2(\chi')^2 \sim -4(\xi - \xi_s)^{-1} \quad \text{as } \xi \rightarrow \xi_s, \quad (26)$$

which may be rearranged to give

$$\chi \sim \frac{4i}{c_\epsilon} (\xi - \xi_s)^{1/2} \quad \text{as } \xi \rightarrow \xi_s. \quad (27)$$

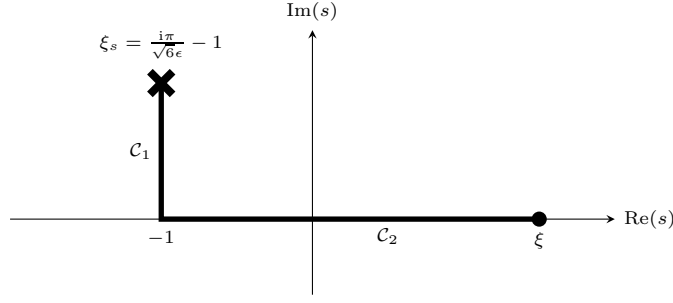


Figure 3: The integral contour for (24), which connects the singularity location $s = \xi_s$ with $s = \xi$. The location of the singularity is denoted by a cross, while the contour is a thick black line. The integral contour may be divided into a vertical component \mathcal{C}_1 and a horizontal component \mathcal{C}_2 . The integral contribution along \mathcal{C}_1 is real, and the integral contribution along \mathcal{C}_2 is imaginary; this implies that $\text{Re}(\chi)$ is constant for real-valued ξ .

3.2.2 Calculating Z and α

Matching (22) at $\mathcal{O}(z_{r-1/2})$, after some simplification,

$$2\chi'Z' + \chi''Z = 0. \quad (28)$$

This expression may be integrated to give

$$Z = \frac{\Lambda}{\sqrt{\chi'(\xi)}}, \quad (29)$$

where Λ is an arbitrary constant that one may determine by considering an inner expansion of the solution in the neighbourhood of $\xi = \xi_s$, and matching the outer limit of this expansion with the inner limit of the late-order ansatz (21). Performing this inner analysis requires the value of α from (21).

To determine α , we use (27) and (29) to find a local expression for Z . Direct computation gives

$$Z \sim \frac{\Lambda c_\epsilon^{1/2}}{2^{1/2}} (\xi - \xi_s)^{1/4} \quad \text{as } \xi \rightarrow \xi_s. \quad (30)$$

By comparing this expression with the local form of the late-order ansatz, we see that

$$z_r(\xi) \sim \frac{\Lambda c_\epsilon^{1/2} (\xi - \xi_s)^{1/4} \Gamma(2r + \gamma)}{2^{1/2} (4i(\xi - \xi_s)^{1/2}/c_\epsilon)^{2r + \alpha}} \quad \text{as } r \rightarrow \infty, \xi \rightarrow \xi_s. \quad (31)$$

In order for this equation to be consistent with the initial behaviour, which has singularity strength of one at $\xi = \xi_s$, we require that $\alpha/2 - 1/4 = 1$, which gives $\alpha = 5/2$.

Using this value of α , as well as local expressions for χ and Z from (27) and (30) respectively, we may perform a local analysis to determine z_r in the neighbourhood of $\xi = \xi_s$, and apply asymptotic matching in order to determine the unknown Λ . The detailed local analysis is presented in Appendix A, and yields $\Lambda = 8\sqrt{\pi i}/c_\epsilon$.

We have now fully determined the late-order ansatz form for z_r , given in (21), and know that

$$z_r(\xi) \sim \frac{8\sqrt{\pi i} \Gamma(2r + 5/2)}{c_\epsilon \sqrt{\chi'(\xi)} \chi(\xi)^{2r + 5/2}} \quad \text{as } r \rightarrow \infty, \quad (32)$$

where χ is given by (24) with the positive choice of sign.

4 Exponential Asymptotics

The main idea of exponential asymptotics is that one can truncate a divergent asymptotic series optimally at some term number N_{opt} such that the remainder is exponentially small in size. The truncated series can be

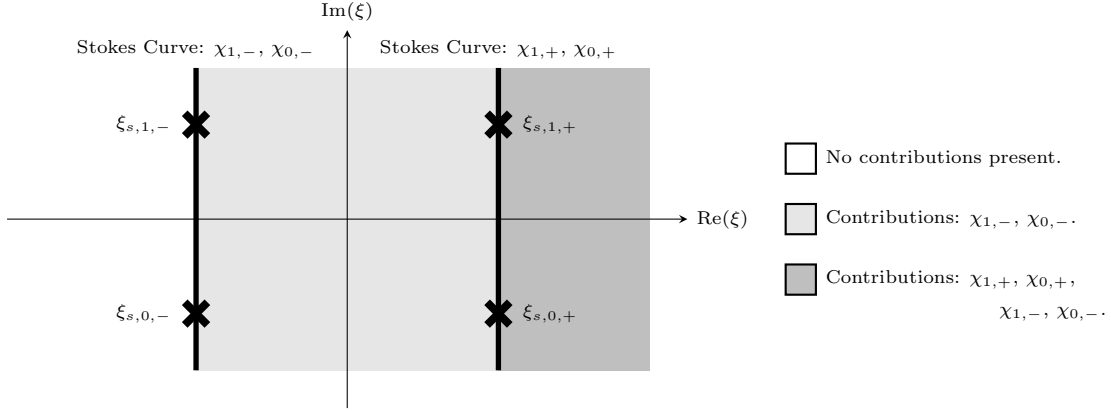


Figure 4: Stokes structure for $z(\xi)$. The Stokes curves are represented as black lines, which originate at the singularities of $z_0(\xi)$ (denoted by crosses). The wave front is located at $\xi = 0$, while $\xi < 0$ corresponds to the region ahead of the travelling wave. We expect the solution to be undisturbed far ahead of the wave, as $\xi \rightarrow -\infty$. Exponentially small oscillations are switched on as each Stokes curve is crossed from left to right. In the light gray region, oscillatory contributions caused by the singularities at $\xi = \xi_{s,1,-}$ and $\xi = \xi_{s,0,-}$ are present in the asymptotic solution. In the darker gray region, oscillatory contributions caused by all four singularities are present in the asymptotic solution.

expressed as

$$y(\xi) = \sum_{r=0}^{N_{\text{opt}}-1} \delta^{2r} y_r(\xi) + y_{\text{exp}}(\xi), \quad z(\xi) = \sum_{j=0}^{N_{\text{opt}}-1} \delta^{2r} z_r(\xi) + z_{\text{exp}}(\xi). \quad (33)$$

where y_{exp} and z_{exp} are exponentially small in the limit $\delta \rightarrow 0$.

4.1 Stokes Structure

We recall that there are four exponentially small asymptotic contributions, associated with the singularities depicted in Figure 2. We denote the corresponding singulants as $\chi_{1,-}$, $\chi_{0,-}$, $\chi_{1,+}$ and $\chi_{0,+}$.

Recall from Section 1.1 that Stokes curves are curves in the complex plane that correspond to $\text{Im}(\chi) = 0$ and $\text{Re}(\chi) > 0$. This means that the Stokes structure may be fully determined from the form of (24), as well as the corresponding singulant equation for the three remaining singularity contributions of interest. In each case, the Stokes curves extend vertically from the singularities of $z_0(\xi)$. This is depicted in Figure 4.

We prescribe that the behaviour preceding the wave front is undistributed, and hence conclude that z_{exp} is zero as $\xi \rightarrow -\infty$. We therefore conclude that the four exponentially small contributions to z_{exp} are present to the right of the corresponding Stokes curves, and therefore are only present in the wake of the leading-order travelling wave.

4.2 Remainder Calculations

Finally, we may determine the form of the contributions that are switched on as the Stokes curves are crossed. In order to accomplish this, we truncate the asymptotic series after N terms, giving

$$y(\xi) = \sum_{r=0}^{N-1} \delta^{2r} y_r(\xi) + S_N(\xi), \quad z(\xi) = \sum_{j=0}^{N-1} \delta^{2r} z_r(\xi) + R_N(\xi), \quad (34)$$

where S_N and R_N are the remainders obtained by truncating the series after N terms. If N is chosen optimally, these remainder terms are exponentially small [4]. We may then analyse these remainder terms in a neighbourhood of the Stokes curves in order to determine the exponentially small asymptotic contributions to the solution behaviour obtained as the Stokes curves are crossed.

In many places, the subsequent analysis is nearly identical to [30], and hence we omit some intermediate technical details. The reader may refer to [30] for a more detailed presentation of the asymptotic analysis contained in this section, or more general descriptions of the technique described in [12, 32].

To optimally truncate the series, we apply the heuristic described in [10], and determine the optimal truncation point by finding the point at which consecutive terms in the series are equal in size. This heuristic gives $N_{\text{opt}} = |\chi|/2\delta + \omega$, where we choose $\omega \in [0, 1)$ in a way that ensures that N_{opt} is an integer. We note that $N_{\text{opt}} \rightarrow \infty$ as $\delta \rightarrow 0$, as expected.

We now apply the truncated series expression to the governing equation. Using the recursion relation to simplify the result, we obtain as $\delta \rightarrow 0$ that

$$c_\epsilon^2 S_N''(\xi) \sim (R_N(\xi + 1) + R_N(\xi - 1))(1 + 2y_0(\xi + 2) - 2y_0(\xi)) \quad (35)$$

$$- (R_N(\xi + 1) + R_N(\xi - 1))(1 + y_0(\xi) - y_0(\xi - 2)) + \dots,$$

$$c_\epsilon^2 \delta^2 R_N''(\xi) + 2(1 + 2y_0(\xi + 1) - 2y_0(\xi - 1))R_N(\xi) \sim -c^2 \delta^{2N} z_{N-1}''(\xi) + \dots, \quad (36)$$

where the terms that we omitted are smaller in magnitude than those that we retained by a factor of δ or more in the limit that $\delta \rightarrow 0$. Throughout the remainder of this section, the asymptotic limit under consideration is $\delta \rightarrow 0$, which will be omitted for simplicity.

Assuming the truncation point occurs after a sufficiently large number of terms, we may apply the expression for the singulant and the late-order term ansatz to (36) to obtain

$$\delta^2 R_N''(\xi) - \chi'(\xi)^2 R_N(\xi) \sim -\frac{\delta^{2N} \chi'(\xi)^2 V(\xi) \Gamma(2N + 5/2)}{\chi(\xi)^{2N+5/2}}. \quad (37)$$

Outside of a region in the neighbourhood of the Stokes curve, the right-hand side of this expression is exponentially small. A Green-Liouville (or WKBJ) analysis outside of this neighbourhood shows that away from Stokes curves, the remainder takes the form $R_N \sim CVe^{-\chi/\delta}$ as $\delta \rightarrow 0$, where C is an arbitrary constant. In order to capture the variation in the neighbourhood of the Stokes curve, we write

$$R_N \sim A(\xi)V(\xi)e^{-\chi(\xi)/\delta}, \quad (38)$$

where $A(\xi)$ is a Stokes switching parameter that varies rapidly near the Stokes curve. Applying this expression to (37) and simplifying gives

$$-2A'\chi'e^{-\chi/\delta} \sim -\frac{\delta^{2N-1}(\chi')^2\Gamma(2N+5/2)}{\chi^{2N+5/2}}, \quad (39)$$

We write this using χ as an independent variable. Noting that $A'(\xi) = \chi'(\xi) \frac{dA}{d\chi}$ and rearranging gives

$$\frac{dA}{d\chi} \sim \frac{\delta^{2N-1}\Gamma(2N+5/2)}{2\chi^{2N+5/2}}e^{\chi/\delta}. \quad (40)$$

We define polar coordinates ($\chi = re^{i\theta}$) and consider only variation that occurs in the angular direction. Applying the optimal truncation $N = N_{\text{opt}}$, and using an asymptotic expansion for the gamma function [16] subsequently gives

$$\frac{dA}{d\theta} \sim i\delta\sqrt{\frac{\pi r}{2}} \exp\left(\frac{r}{\sqrt{\delta}}(e^{i\theta} - 1) - \frac{i\theta r}{\sqrt{\delta}} + i\theta(1 - 5/2 - 2\omega)\right). \quad (41)$$

The right-hand side of this expression is exponentially small in δ , except in the neighborhood of $\theta = 0$. We therefore define an inner region $\theta = \delta^{1/2}\bar{\theta}$ and thereby find that

$$\frac{dA}{d\bar{\theta}} \sim i\delta^{3/2}\sqrt{\frac{\pi r}{2}}e^{-r\bar{\theta}^2/2}. \quad (42)$$

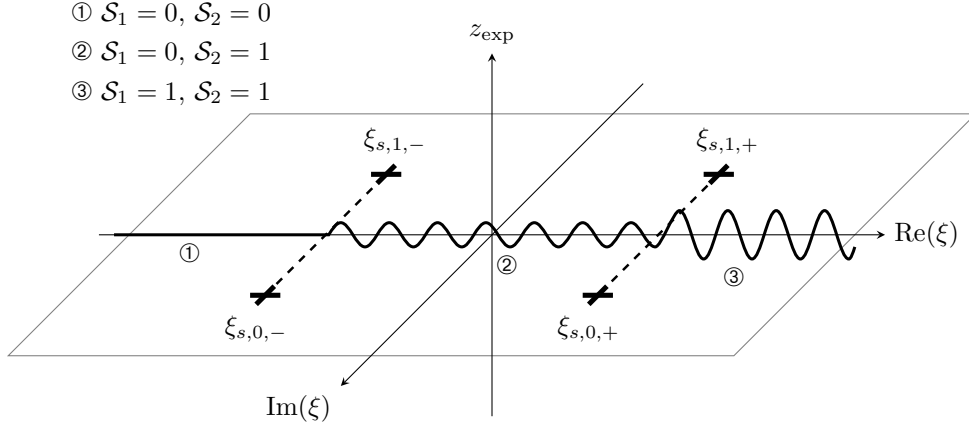


Figure 5: Behavior of the asymptotic coefficients as the Stokes curves are crossed and a schematic illustration of the associated exponentially small contribution. Recall that if $\xi \in \mathbb{R}$, then $\xi < 0$ corresponds to $n > c_\epsilon t$, which describes the undisturbed region ahead of the wave; in contrast, $\xi > 0$ corresponds to $n < c_\epsilon t$, which describes the region in the wake of the wave. In the first region, both of the multipliers are zero, and there are no oscillations. As one crosses the Stokes curve along $\text{Re}(\xi) = -1$, the coefficient \mathcal{S}_1 changes rapidly from 0 to 1. As one crosses the Stokes curve across $\text{Re}(\xi) = 1$, the coefficient \mathcal{S}_2 varies rapidly from 0 to 1, ensuring that all four contributions are present in the third region.

Consequently, by integration, we see that the behavior as the Stokes curve is crossed is

$$A \sim i\delta^{3/2} \sqrt{\frac{\pi r}{2}} \int_{-\infty}^{\bar{\theta}} e^{-rs^2/2} ds \quad \text{as } \delta \rightarrow 0. \quad (43)$$

Therefore, converting back to outer coordinates, as the Stokes curve is crossed from $\theta < 0$ to $\theta > 0$, we find that $[A]_{-}^{\pm} \sim \pi i \delta^{3/2}$ as $\delta \rightarrow 0$, where we use the notation $[f]_{-}^{\pm}$ to describe the change in a function f as the Stokes curve is crossed from $\theta < 0$ to $\theta > 0$. Because $R_N(\xi)$ must be 0 ahead of the solitary wave (i.e., when $\text{Im}(\chi) < 0$), we find from (38) that behind the wave front, the exponentially small contribution is given in $\delta \rightarrow 0$ limit by

$$R_N \sim \frac{\pi \mathcal{S}(\xi) \Lambda i \delta^{3/2}}{\sqrt{\chi'(\xi)}} e^{-\chi(\xi)/\delta} \quad \text{as } \delta \rightarrow 0. \quad (44)$$

where \mathcal{S} varies rapidly from 0 to 1 in the neighborhood of the Stokes curve.

We recall that there are four relevant exponentially small contributions, associated with each of the four singularities in Figure 2. The contributions associated with $\chi_{0,-}$ and $\chi_{0,+}$ are the complex conjugates of those associated with $\chi_{1,-}$ and $\chi_{1,+}$ respectively. We consequently find that the exponentially small contribution to the asymptotic behaviour in the wake of the solitary wave is given by

$$z_{\text{exp}} \sim \left[\frac{\pi \mathcal{S}_1(\xi) \Lambda i \delta^{3/2}}{\sqrt{\chi'_{1,-}(\xi)}} e^{-\chi_{1,-}(\xi)/\delta} + \frac{\pi \mathcal{S}_2(\xi) \Lambda i \delta^{3/2}}{\sqrt{\chi'_{1,+}(\xi)}} e^{-\chi_{1,+}(\xi)/\delta} \right] + \text{c.c.} \quad \text{as } \delta \rightarrow 0, \quad (45)$$

where \mathcal{S}_1 varies from zero to one in the neighbourhood of the Stokes curve that follows $\text{Re}(\xi) = -1$, \mathcal{S}_2 varies from zero to one in the neighbourhood of the Stokes curve that follows $\text{Re}(\xi) = 1$, and c.c. denotes the complex conjugate. The behaviour of these coefficients is illustrated in Figure 5.

Noting that $\chi'_{1,-}(\xi) = \chi'_{1,+}(\xi)$, we simplify this to give

$$z_{\text{exp}}(\xi) \sim \frac{\pi \Lambda i \delta^{3/2}}{\sqrt{\chi'_{1,-}(\xi)}} \left[\mathcal{S}_1(\xi) e^{-\chi_{1,-}(\xi)/\delta} + \mathcal{S}_2(\xi) e^{-\chi_{1,+}(\xi)/\delta} \right] + \text{c.c.} \quad \text{as } \delta \rightarrow 0, \quad (46)$$

where $\chi_{1,-}$ is given by the integral (24), and can be approximated in the long-wave limit using the value of $y_0(\xi)$ given in (16). The value of $\chi_{1,+}$ can be written as an integral and approximated in near-identical fashion.

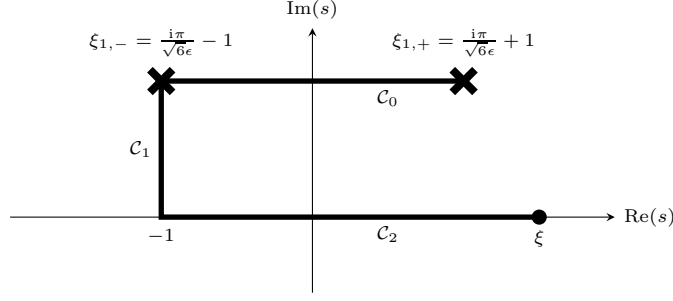


Figure 6: The integral contour for (24), which connects the singularity location $s = \xi_{1,+}$ with $s = \xi$. The location of the singularity is denoted by a cross, while the contour is a thick black line. The integral contour is deformed to pass through $s = \xi_{1,-}$. It may be divided into a vertical component C_1 and two horizontal components, C_0 and C_2 . The integral contribution along C_1 is real, and the integral contributions along C_0 and C_2 are imaginary; this implies that $\text{Re}(\chi_{1,+})$ is constant for real-valued ξ , and identical to the real part of $\text{Re}(\chi_{1,-})$.

Using the remainder equations (35)–(36), we can also show that

$$y_{\text{exp}}(\xi) \sim -\frac{\pi\Lambda i\delta^{5/2}}{2c_\epsilon^2\sqrt{\chi'_{1,-}(\xi+1)}} \left[\mathcal{S}_1(\xi+1)e^{-\chi_{1,-}(\xi+1)/\delta} + \mathcal{S}_2(\xi+1)e^{-\chi_{1,+}(\xi+1)/\delta} \right] \\ -\frac{\pi\Lambda i\delta^{5/2}}{2c_\epsilon^2\sqrt{\chi'_{1,-}(\xi-1)}} \left[\mathcal{S}_1(\xi-1)e^{-\chi_{1,-}(\xi-1)/\delta} + \mathcal{S}_2(\xi-1)e^{-\chi_{1,+}(\xi-1)/\delta} \right] + \text{c.c.} \quad \text{as } \delta \rightarrow 0. \quad (47)$$

Consequently, we have obtained an asymptotic description for the exponentially small far-field oscillations present in the travelling wave solution to (1) in the small mass ratio limit.

4.3 Far-field oscillations

It is possible to use (23) to simplify the form of z_{exp} in the far field, corresponding to $|\xi| \rightarrow \infty$. We note that that $y_0(\xi+1) - y_0(\xi-1)$ decays exponentially in this limit, as the leading-order solution is known to be a true solitary wave. This implies that $\chi' \sim i\sqrt{2}/c_\epsilon$ as $|\xi| \rightarrow \infty$.

Additionally, we see from contour deformation that $\text{Re}(\chi_{1,-}) = \text{Re}(\chi_{1,+})$, and that this quantity is constant for both singulants. This is determined by deforming the contour for $\chi_{1,+}$ to that depicted in Figure 6. Integrating χ' along contours C_0 and C_2 produces imaginary contributions, while integrating along C_1 produces the same real contribution as $\chi_{1,-}$. This can be confirmed by comparing the contours in Figure 3 and Figure 6, and noting that the integrand is identical in both cases.

Using these simplifications, we find that in the far-field where both Stokes multipliers are active, the asymptotic behaviour of the system simplifies to

$$z_{\text{exp}}(\xi) \sim \frac{\pi\Lambda\sqrt{ic_\epsilon}\delta^{3/2}}{2^{1/4}} e^{-\text{Re}(\chi_{1,-})/\delta} \left[e^{-i\text{Im}(\chi_{1,-}(\xi))/\delta} + e^{-i\text{Im}(\chi_{1,+}(\xi))/\delta} \right] + \text{c.c.} \quad \text{as } \delta \rightarrow 0. \quad (48)$$

Using the result that $\Lambda = 8\sqrt{\pi i}/c_\epsilon$ and simplifying gives

$$z_{\text{exp}}(\xi) \sim \frac{16\pi^{3/2}\delta^{3/2}}{c_\epsilon^{1/2}2^{1/4}} e^{-\text{Re}(\chi_{1,-})/\delta} \left[\sin\left(\frac{\text{Im}(\chi_{1,-}(\xi))}{\delta}\right) + \sin\left(\frac{\text{Im}(\chi_{1,+}(\xi))}{\delta}\right) \right] \quad \text{as } \delta \rightarrow 0. \quad (49)$$

Recall that $\chi' \sim i\sqrt{2}/c_\epsilon$ as $\xi \rightarrow \infty$. We therefore write (49) in the convenient form

$$z_{\text{exp}}(\xi) \sim \frac{16\pi^{3/2}\delta^{3/2}}{c_\epsilon^{1/2}2^{1/4}} e^{-\text{Re}(\chi_{1,-})/\delta} \left[\sin\left(\frac{\sqrt{2}\xi}{\delta c_\epsilon} + \phi_{1,-}\right) + \sin\left(\frac{\sqrt{2}\xi}{\delta c_\epsilon} + \phi_{1,+}\right) \right] \quad \text{as } \delta \rightarrow 0, \quad (50)$$

where $\phi_{1,\pm}$ is a constant phase offset. It is straightforward to find a similar expression for y_{exp} in near-identical fashion.

We see that z_{exp} contains two non-decaying wavetrains as $\xi \rightarrow \infty$. These wave trains have high frequency and identical exponentially small amplitude in the limit that $\delta \rightarrow 0$. Calculating the phase offsets of the wavetrains requires direct evaluation of the integral (24), and plays an important role in finding the orthogonality condition in Section 6. Finding the orthogonality condition amounts to determining mass ratios that produce phase offsets for which the two wavetrains interfere destructively, eliminating the far-field oscillations.

5 Numerical comparisons

In order to determine the utility of the asymptotic description of far-field oscillations in (46), we compare the amplitude predicted by the asymptotic analysis with a numerical study of the diatomic FPUT travelling wave.

The numerical method was implemented in MATLAB using an implementation of the fourth-order Runge Kutta algorithm (RK4). Rather than computing the particle positions directly, the implementation computed the quantities $r(n,t)$ and $p(n,t)$ described in (5). The particle positions $y(n,t)$ and $z(n,t)$ were obtained by inverting the relationship between these quantities. This implementation was chosen because the leading-order behaviours $r_0(n,t)$ and $p_0(n,t)$ are both zero in the far field, which is computationally convenient. The initial conditions were chosen to be $r(n,0) = r_0(n,0)$ and $p(n,0) = p_0(n,0)$.

The domain was restricted to include $M = 2^{12}$ particles with indices given by $-M/2 + 1 \leq n \leq M/2$, with periodic boundary conditions. The initial condition was given by the leading-order travelling wave solution (16), and the time step was chosen to be $h = 1/40$. In order to prevent interactions between the far-field oscillations and the leading-order travelling wave as it returns to its original position, a window function was applied to the solution. This involved multiplying $r(n,t)$ and $p(n,t)$ by a function $W(n - n_{\text{front}} + M/8)$, where

$$W(k) = \begin{cases} 1, & |k| \leq \frac{5N}{16}, \\ 1 - \frac{8}{N}(|k| - \frac{5N}{16}), & \frac{5N}{16} < |k| \leq \frac{7N}{16}, \\ 0, & \frac{7N}{16} < |k| \leq \frac{N}{2}. \end{cases} \quad (51)$$

This results in the numerical algorithm not conserving energy; however, this did not cause problems for the algorithm, which was still able to obtain the exponentially small oscillations after transient effects in the system dissipated. In order to eliminate transient effects, the computations were run for $0 < t < t_{\text{max}}$, where typical values of the maximum time t_{max} were chosen to be between 10^5 and 10^6 , depending on the time required for transient effects to vanish.

The results of this numerical method are illustrated in Figure 7, in which they are compared to the asymptotic prediction (46). It was numerically challenging to determine wave amplitudes for values of δ smaller than those presented in Figure 7. We see that the asymptotic method does capture the qualitative behaviour predicted by the numerical simulations in the region available for comparison.

While it is challenging to extend the computations to smaller values of δ , it is hoped that smaller values of δ would correspond to more accurate approximations, as in the case of the diatomic Toda lattice [30]; however, this could not be shown conclusively without a more accurate numerical study. It can be seen from the larger values of δ represented in Figure 7 (particular for $\epsilon = 0.25$ and $\epsilon = 0.3$) that the asymptotic approximation becomes qualitatively and quantitatively inaccurate for values of δ that are not particularly small, as is expected.

There is error introduced into the asymptotic solution by the fact that the leading-order solution (8) is an approximation that depends on a small parameter ϵ , and we expect this to introduce an additional source of error to the asymptotic expansion. Naively, we would expect this error to vary straightforwardly in ϵ , decreasing as $\epsilon \rightarrow 0$; however, from comparing the asymptotic and numeric results, it appears there is exists more complicated nonlinear interaction between the asymptotic error in ϵ and δ .

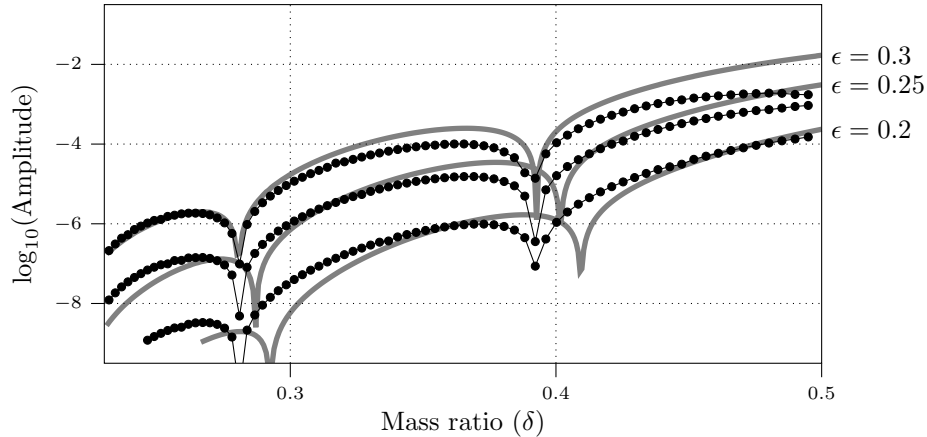


Figure 7: Amplitude of the far-field oscillations given by the remainder expression z_{exp} in (46) for a range of values of δ , compared to numerical computations. The thick grey curves represent the amplitude predicted by the leading-order exponentially small behavior z_{exp} , and the filled circles represent the amplitude obtained using numerical simulations. It is clear that the asymptotic and numerical solutions have the same qualitative behaviour, and are a reasonable quantitative match. For smaller values of δ than those depicted, it became challenging to isolate the oscillatory behaviour within the computation time window. In the solutions, there clearly exist values of δ that result in wave cancellation (corresponding to zero values of the amplitude).

Importantly, we see that both the numerical and asymptotic results predict the existence of mass ratios that cause the leading-order oscillations to cancel entirely, leading to truly localized solitary wave solutions. This corresponds to predictions made in [30] about the diatomic Toda lattice. We will study these points in more detail in Section 6.

Finally, by looking at individual numerical solutions, we see that sampling the very high frequency sinusoidal term at regular intervals often introduces slower periodic effects into the wave train that are not obvious from the asymptotic form given in (46). This is shown schematically in Figure 8 (a), representing an example $r(j, t)$ sampled at a particular time. In this schematic, the solid gray curve represents the full solution $r(\xi) = r(j - c_\epsilon t)$, where ξ is a continuous variable, while the filled circles represent the sampled points for integer values of j at fixed time $t = t_s$. The fast sinusoidally varying oscillations described in (46) are sampled by the discrete chain at regular intervals; as the sampling period is generally not an exact multiple of the sinusoid period, this can introduce slower periodic effects into the solution related to the interaction between the two periodicities.

The numerical wave train in Figure 8 (b) illustrates visible periodic effects introduced by sampling, while the wave train in Figure 8 (c) contains more complicated periodic effects. In both cases, it is still possible to calculate the amplitude of the underlying continuous waveform, although care must be taken in order to measure this quantity numerically. This sampling also explains the relationship between the results obtained in this study and the periodic effects seen in the numerically-computed wave trains in [23].

6 Orthogonality Condition

It is apparent in Figure 7 that there are particular values of δ which cause the far-field oscillation amplitude to vanish, due to destructive interference between the exponentially small oscillations. As the two wave trains in z_{exp} given in (46) have identical amplitude, it is possible to select parameter values so that the waves precisely cancel each other out. Such configurations produce genuinely localized solitary waves, even at exponentially small orders. Systems with these particular parameter values are said (for example, in [25, 26]) to satisfy an ‘anti-resonance’ condition.

This behaviour was seen in the diatomic Toda lattice [30], and it is possible to show that corresponding

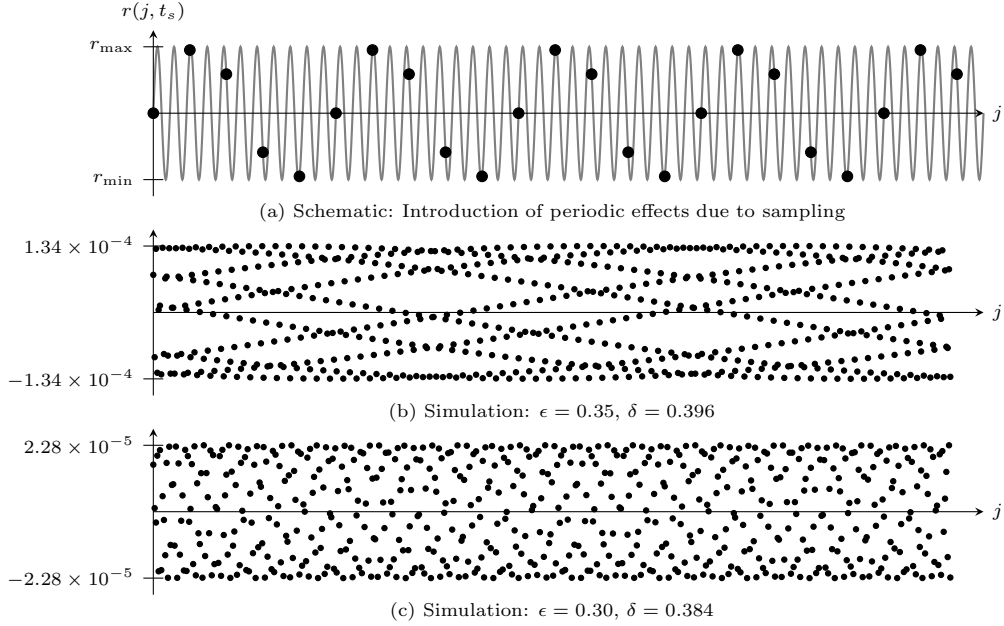


Figure 8: Schematic (a) illustrates how periodic effects may appear in regular sampling of fast oscillatory solutions. In this case, the high-frequency continuous gray curve is sampled at regular intervals, indicated by filled black circles. The effect of this sampling is to introduce a slower periodic component into the sampled solution. Figures (b) and (c) show numerically computed wave trains for different values of ϵ and δ . In (b), there are obvious periodic effects introduced by sampling the high-frequency wave train, but the periodic sampling effects introduced in (c) are less immediately apparent.

behaviour is present in asymptotic solutions the diatomic FPUT lattice. We note that in the wake of the wave front, when all oscillatory contributions are present, the exponentially small contribution is given by

$$z_{\text{exp}} \sim \frac{\pi \Lambda i \delta^{3/2}}{\sqrt{\chi'_{1,-}(\xi)}} \left[e^{-\chi_{1,-}(\xi)/\delta} + e^{-\chi_{1,+}(\xi)/\delta} \right] + \text{c.c.} \quad \text{as } \delta \rightarrow 0. \quad (52)$$

It is clear that destructive interference occurs if

$$e^{-\chi_{1,-}(\xi)/\delta} + e^{-\chi_{1,+}(\xi)/\delta} = 0. \quad (53)$$

We refer to this condition as an ‘orthogonality condition’. We can simplify this condition by writing the singulant as

$$\chi_{1,+} = \int_{\xi_{1,+}}^{\xi_{1,-}} \chi'(s) ds + \chi_{1,-} = \lambda + \chi_{1,-}. \quad (54)$$

This is a consequence of comparing the contour for $\chi_{1,+}$ shown in Figure 6 with the contour for $\chi_{1,-}$ shown in Figure 3. The orthogonality condition (53) now simplifies to give

$$1 + e^{-\lambda/\delta} = 0. \quad (55)$$

This gives the condition $\lambda/\delta = (2K + 1)\pi i$, for $K \in \mathbb{Z}$, or

$$\delta = \frac{\sqrt{2}}{(2K + 1)\pi c_\epsilon} \int_{\xi_{1,+}}^{\xi_{1,-}} \sqrt{1 + y_0(\xi + 1) - y_0(\xi - 1)} ds, \quad (56)$$

which can be approximated in the long-wave limit as

$$\delta \approx \frac{1}{(2K + 1)\pi} \int_{\pi i/\sqrt{6}\epsilon - 1}^{\pi i/\sqrt{6}\epsilon + 1} \sqrt{1 + \sqrt{6}\epsilon \tanh\left(\sqrt{\frac{3}{2}}\epsilon(\xi + 1)\right) - \sqrt{6}\epsilon \tanh\left(\sqrt{\frac{3}{2}}\epsilon(\xi - 1)\right)} ds, \quad K \in \mathbb{R}. \quad (57)$$

K	Computed δ	Asymptotic δ
2	0.3922	0.4258
3	0.2809	0.3041
4	0.2248	0.2365
5	0.1932	0.1935
6	0.1677	0.1638

Table 1: Comparison between δ values for nanopteron-free solutions computed with $\epsilon = 0.25$, and the asymptotic prediction obtained from (57) for corresponding values of K . The asymptotic prediction provides a good approximation for the numerically-obtained solutions. As in the amplitude predictions, this is not as accurate as the predictions for the diatomic Toda lattice from [30], even for larger values of K (and hence smaller values of δ).

While this integral does not have a convenient solution like the corresponding integral in the Toda problem in [30], it is straightforward to show that the integrand is real along the integral contour between the two singular points, and consequently that the result of the integral is real-valued. This therefore gives a set of real values for δ at which the far-field oscillations vanish.

In Table 1, asymptotic predictions of the values of δ that cause the far-field oscillations to cancel are compared with numerical predictions. These numerical predictions were found using the methods from Section 5, however the size of the time steps were decreased in size, and the maximum simulation time was increased in order to resolve the waves at smaller values of δ than those presented in Figure 7. This allowed us to determine the values of δ corresponding to $K = 2, \dots, 6$.

It is clear from Table 1 that the asymptotic predictions of nanopteron-free values of δ may be accurately predicted using the asymptotic form of z_{exp} .

7 Discussion and Conclusions

In this study, we considered travelling slightly supersonic wave behaviour in a diatomic FPUT lattice with small mass ratio. The asymptotic solutions of this system are nanoptera, or solitary-wave solutions that are not exponentially localized, but instead possess non-decaying trains of oscillations in the far field behind the wave front. These oscillations are exponentially small, so their dynamics are invisible to ordinary asymptotic power-series approaches. The existence of these oscillations was previously proven in [17].

In this study, we demonstrated that far-field oscillations ‘switch on’ across special curves in the complex plane known as Stokes curves, which originate at singularities in the analytic continuation of the leading-order behaviour. The far field oscillations present in the asymptotic wave behaviour are therefore a consequence of Stokes Phenomenon. We derived asymptotic forms for these exponentially small oscillations, given in (46) and (47), as well as a simplified expression for the behaviour of the oscillations far from the wave front 50. We compared the results of this analysis to numerical studies, and found that the asymptotic results were useful for predicting both the amplitude of the oscillations as well as the special mass ratios that produce localized solitary wave solutions.

One significant difference between the travelling wave solutions in the diatomic FPUT lattice as opposed to the previous analysis of the diatomic Toda lattice is that the leading order solution could not be determined exactly for the diatomic FPUT approximation, but was instead approximated using the long-wave limit approximation from [22]. This change introduced a second small parameter into the problem; however, with careful treatment, it was still possible to determine the leading-order behaviour of the late-order terms. This work establishes the effectiveness of exponential asymptotics for determining asymptotic nanopteron solutions in other lattice systems for which the leading-order behaviour must be approximated, such as the diatomic Hertzian lattice [34], the woodpile lattice [29], or lattices of resonant granular crystals [40].

By isolating the exponentially small terms, we found an asymptotic condition that predicted the wave trains would cancel entirely, given in (57). If this condition is satisfied, the solutions do not possess a wave train in the wake of the travelling wave front; instead, they consist of a localized solitary wave. Similar results were found using an exponential asymptotic analysis on the diatomic Toda lattice in [30], as well as other studies in which special choices of mass ratios and wave parameters produce localized solitary wave solutions [25, 28, 41]. Importantly, as in the diatomic Toda lattice from [30], this orthogonality condition arises as a consequence of Stokes Phenomenon, and the precise cancellation of exponentially small wave trains that appear as two different Stokes curves are crossed.

It is important to emphasise that the solution that we discussed in this paper is a formal solution asymptotic solution, and we did not supply a rigorous proof of these results. Faver & Wright [18] used rigorous estimates for the local leading-order solitary wave to prove the existence of the exponentially small oscillations in a nanopteron solution of FPUT systems. Typically, exponential asymptotic arguments can be made rigorous using the method of Borel transforms in order to replace the divergent tail of the asymptotic series with a quantity that can be bounded rigorously. This is beyond the scope of the present work; however, examples of rigorous exponential asymptotic bounding may be found in, for example, [2, 7, 6, 14] and others.

8 Acknowledgements

CJL thanks Prof. J. Douglas Wright for helpful discussions on the implementation of the numerical methods applied in Section 5, and Dr Justin Tzou for discussions about the manuscript. CJL is supported by ARC Discovery Project DP190101190.

References

- [1] J. T. Beale, *Exact solitary water waves with capillary ripples at infinity*, Comm. Pure Appl. Math. **44** (1991), no. 2, 211–257.
- [2] T. Bennett, C. J. Howls, G. Nemes, and A. B. Olde Daalhuis, *Globally exact asymptotics for integrals with arbitrary order saddles*, SIAM Journal on Mathematical Analysis **50** (2018), no. 2, 2144–2177.
- [3] M. V. Berry, *Stokes phenomenon; smoothing a Victorian discontinuity*, Pub. Math. de L’IHÉS **68** (1988), 211–221.
- [4] ———, *Uniform asymptotic smoothing of Stokes’s discontinuities*, Proc. Roy. Soc. Lond. A **422** (1989), no. 1862, 7–21.
- [5] ———, *Asymptotics, superasymptotics, hyperasymptotics*, Asymptotics Beyond All Orders (H. Segur, S. Tanveer, and H. Levine, eds.), Plenum, Amsterdam, 1991, pp. 1–14.
- [6] M. V. Berry and C. J. Howls, *Hyperasymptotics*, Proc. Roy. Soc. Lond. A **430** (1990), no. 1880, 653–668.
- [7] ———, *Hyperasymptotics for integrals with saddles*, Proc. Roy. Soc. Lond. A **434** (1991), no. 1892, 657–675.
- [8] J. P. Boyd, *A numerical calculation of a weakly non-local solitary wave: the ϕ^4 breather*, Nonlinearity **3** (1990), no. 1, 177–195.
- [9] ———, *Weakly nonlocal solitary waves and beyond-all-orders asymptotics: Generalized solitons and hyperasymptotic perturbation theory*, Mathematics and Its Applications, vol. 442, Kluwer, Amsterdam, 1998.
- [10] ———, *The devil’s invention: Asymptotic, superasymptotic and hyperasymptotic series*, Acta Appl. Math. **56** (1999), no. 1, 1–98.

- [11] ———, *Hyperasymptotics and the linear boundary layer problem: Why asymptotic series diverge*, SIAM Rev. **47** (2005), no. 3, 553–575.
- [12] S. J. Chapman, J. R. King, and K. L. Adams, *Exponential asymptotics and Stokes lines in nonlinear ordinary differential equations*, Proc. Roy. Soc. Lond. A **454** (1998), no. 1978, 2733–2755.
- [13] M. Chirilus-Bruckner, C. Chong, O. Prill, and G. Schneider, *Rigorous description of macroscopic wave packets in infinite periodic chains of coupled oscillators by modulation equations*, Discrete Contin. Dyn. Syst. Ser. S **5** (2012), no. 5, 879–901.
- [14] O. Costin, *Asymptotics and Borel summability*, Chapman and Hall/CRC, 2008.
- [15] R. B. Dingle, *Asymptotic expansions: Their derivation and interpretation*, Academic Press, New York, 1973.
- [16] *NIST Digital Library of Mathematical Functions*, <http://dlmf.nist.gov/>, Release 1.0.22 of 2019-03-15, F. W. J. Olver, A. B. Olde Daalhuis, D. W. Lozier, B. I. Schneider, R. F. Boisvert, C. W. Clark, B. R. Miller and B. V. Saunders, eds.
- [17] T. E. Faver, *Nanopteron-stegoton traveling waves in spring dimer Fermi-Pasta-Ulam-Tsingou lattices*, arXiv preprint arXiv:1710.07376 (2017).
- [18] T. E. Faver and J. D. Wright, *Exact diatomic Fermi–Pasta–Ulam–Tsingou solitary waves with optical band ripples at infinity*, SIAM J. Math. Anal. **50** (2018), no. 1, 182–250.
- [19] G. Friesecke and R. L. Pego, *Solitary waves on FPU lattices: I. Qualitative properties, renormalization and continuum limit*, Nonlinearity **12** (1999), no. 6, 1601.
- [20] ———, *Solitary waves on FPU lattices: II. Linear implies nonlinear stability*, Nonlinearity **15** (2002), no. 4, 1343.
- [21] G. Friesecke and J. A. D. Wattis, *Existence theorem for solitary waves on lattices*, Comm. Math. Phys. **161** (1994), no. 2, 391–418.
- [22] J. Gaison, S. Moskow, J. D. Wright, and Q. Zhang, *Approximation of polyatomic FPU lattices by KdV equations*, Multiscale Model. Sim. **12** (2014), no. 3, 953–995.
- [23] N. Giardetti, A. Shapiro, S. Windle, and J. D. Wright, *Metastability of solitary waves in diatomic FPUT lattices*, Math. in Eng. **1** (2019), 419.
- [24] A. Hoffman and J. D. Wright, *Nanopteron solutions of diatomic Fermi–Pasta–Ulam–Tsingou lattices with small mass-ratio*, Physica D **358** (2017), 33–59.
- [25] K. R. Jayaprakash, Y. Starosvetsky, and A. F. Vakakis, *New family of solitary waves in granular dimer chains with no precompression*, Phys. Rev. E **83** (2011), no. 3, 036606.
- [26] K. R. Jayaprakash, Y. Starosvetsky, A. F. Vakakis, and O. V. Gendelman, *Nonlinear resonances leading to strong pulse attenuation in granular dimer chains*, J. Nonlinear Sci. **23** (2013), no. 3, 363–392.
- [27] N. Joshi and C. J. Lustri, *Generalized solitary waves in a finite-difference Korteweg-de Vries equation*, Stud. Appl. Math. **142** (2019), no. 3, 359–384.
- [28] P. G. Kevrekidis, A. Stefanov, and H. Xu, *Traveling waves for the mass in mass model of granular chains*, Lett. Math. Phys. (2016), 1–22.

- [29] E. Kim, F. Li, C. Chong, G. Theocharis, J. Yang, and P. G. Kevrekidis, *Highly nonlinear wave propagation in elastic woodpile periodic structures*, Phys. Rev. Lett. **114** (2015), no. 11, 118002.
- [30] C. J. Lustrì and M. A. Porter, *Nanoptera in a period-2 Toda chain*, SIAM J. App. Dyn. Sys. **17** (2018), no. 2, 1182–1212.
- [31] Y. Okada, S. Watanabe, and H. Tanaca, *Solitary wave in periodic nonlinear lattice*, J. Phys. Soc. Jpn. **59** (1990), no. 8, 2647–2658.
- [32] A. B. Olde Daalhuis, S. J. Chapman, J. R. King, J. R. Ockendon, and R. H. Tew, *Stokes phenomenon and matched asymptotic expansions*, SIAM J. App. Math. **55** (1995), no. 6, 1469–1483.
- [33] St. Pnevmatikos, N. Flytzanis, and M. Remoissenet, *Soliton dynamics of nonlinear diatomic lattices*, Phys. Rev. B **33** (1986), 2308–2321.
- [34] M. A. Porter, C. Daraio, I. Szelenowicz, E. B. Herbold, and P. G. Kevrekidis, *Highly nonlinear solitary waves in heterogeneous periodic granular media*, Physica D **238** (2009), no. 6, 666–676.
- [35] W.-X. Qin, *Wave propagation in diatomic lattices*, SIAM J. Math. Anal. **47** (2015), no. 1, 477–497.
- [36] G. Schneider and C. E. Wayne, *Counter-propagating waves on fluid surfaces and the continuum limit of the Fermi-Pasta-Ulam model*, Equadiff 99: (In 2 Volumes), World Scientific, 2000, pp. 390–404.
- [37] G. G. Stokes, *On the discontinuity of arbitrary constants which appear in divergent developments*, Trans. Cam. Phil. Soc. **10** (1864), 106–128.
- [38] Y. Tabata, *Stable solitary wave in diatomic Toda lattice*, J. Phys. Soc. Jpn. **65** (1996), no. 12, 3689–3691.
- [39] A. Vainchtein, Y. Starosvetsky, J. D. Wright, and R. Perline, *Solitary waves in diatomic chains*, Phys. Rev. E **93** (2016), no. 4, 042210.
- [40] K. Vorotnikov, Y. Starosvetsky, G. Theocharis, and P. G. Kevrekidis, *Wave propagation in a strongly nonlinear locally resonant granular crystal*, Physica D **365** (2018), 27–41.
- [41] H. Xu, P. G. Kevrekidis, and A. Stefanov, *Traveling waves and their tails in locally resonant granular systems*, J. Phys. A **48** (2015), no. 19, 195204.
- [42] D. Yong and R. J. LeVeque, *Solitary waves in layered nonlinear media*, SIAM J. Appl. Math. **63** (2003), no. 5, 1539–1560.

A Determining Λ

To determine the value of Λ , we match the late-order expansion in the outer region with the local solution in an inner region near the singularity. Using Van Dyke’s matching principle we match the inner limit as $\xi \rightarrow \xi_s$ of the outer expansion with the outer limit of the inner expansion, determined below.

In the inner region near the singularity at $\xi = \xi_s$, we find that

$$y_0(\xi + 1) \sim \frac{2}{\xi - \xi_s} + \mathcal{O}(\xi - \xi_s), \quad (58)$$

$$y_0(\xi - 1) \sim -\sqrt{6}\epsilon \coth(\sqrt{6}\epsilon) + \mathcal{O}(\xi - \xi_s), \quad (59)$$

$$z_0(\xi) \sim \frac{1}{\xi - \xi_s} - \frac{\sqrt{6}\epsilon}{2} \coth(\sqrt{6}\epsilon) + \mathcal{O}(\xi - \xi_s). \quad (60)$$

In order to locate the inner region, we must determine the region in which the inner analysis breaks down. From the form of the late-order ansatz, we find that this occurs at $\delta^2 \chi^{-2} = \mathcal{O}(1)$ as $\delta \rightarrow 0$, or $\delta^2 (\xi - \xi_s)^{-1} = \mathcal{O}(1)$. This corresponds to the inner scaling $\xi - \xi_s = \delta^2 \bar{\xi}$. The appropriate rescaled inner variables are given by

$$y(\xi + 1) = \frac{2}{\delta^2 \bar{\xi}} + \hat{y}(\bar{\xi} + \delta^{-2}), \quad y(\xi - 1) = \hat{y}(\bar{\xi} - \delta^{-2}), \quad z(\xi) = \frac{1}{\delta^2 \bar{\xi}} + \frac{\hat{z}(\bar{\xi})}{\delta^2}. \quad (61)$$

Retaining the leading-order terms as $\delta \rightarrow 0$ in the rescaled inner equation gives

$$\frac{2}{\bar{\xi}^3} + \frac{d^2 \hat{z}(\bar{\xi})}{d\bar{\xi}^2} = -\frac{4\hat{z}(\bar{\xi})}{c_\epsilon^2 \bar{\xi}}. \quad (62)$$

We express \hat{z} in terms of the local series

$$\hat{z}(\bar{\xi}) \sim \sum_{j=1}^{\infty} \frac{a_j}{\bar{\xi}^{j+1}} \quad \text{as } \bar{\xi} \rightarrow 0, \quad (63)$$

as the term with power $j = 1$ is already built into the inner form of $v(\xi)$. This gives

$$\frac{2}{\bar{\xi}^3} + \sum_{j=1}^{\infty} \frac{(j+1)(j+2)a_j}{\bar{\xi}^{j+3}} = -\frac{4}{c_\epsilon^2} \sum_{j=1}^{\infty} \frac{a_j}{\bar{\xi}^{j+2}}. \quad (64)$$

From matching at leading order, we see that $a_1 = -c_\epsilon^2/2$. At subsequent orders, we obtain the recurrence relation

$$c_\epsilon^2 j(j+1)a_{j-1} = -4a_j. \quad (65)$$

Noting the form of a_1 , this gives

$$a_j = -\frac{c_\epsilon^2}{2} \left(\frac{c_\epsilon^2}{4}\right)^j (-1)^j \Gamma(j+2) \Gamma(j+1). \quad (66)$$

By comparing the series expression with the inner limit of the late-order ansatz, we find using Stirling's formula

$$\Lambda = \frac{2^{1/2}}{c_\epsilon^{1/2}} \lim_{r \rightarrow \infty} \frac{a_r (4i/c_\epsilon)^{2r+5/2}}{\Gamma(2r+5/2)} = \frac{2^{9/2} i^{1/2}}{c_\epsilon} \lim_{r \rightarrow \infty} \frac{4^r \Gamma(r+2) \Gamma(r+1)}{\Gamma(2r+5/2)} = \frac{8\sqrt{\pi} i}{c_\epsilon}. \quad (67)$$